Benchmarking of Vertically-Integrated CO_2 Flow Simulations at the Sleipner Field, North Sea

L.R. Cowton[a,b], J.A. Neufeld[a,b,c,*], N.J. White[a], M.J. Bickle[d], G.A. Williams[e], J.C. White[f], R.A. Chadwick[f]

[a] *Bullard Laboratories, Department of Earth Sciences, University of Cambridge, Madingley Rise, Madingley Road, Cambridge, CB3 0EZ, UK*
[b] *BP Institute, University of Cambridge, Madingley Road, Cambridge, CB3 0EZ, UK*
[c] *Institute of Theoretical Geophysics, Department of Applied Mathematics and Theoretical Physics, University of Cambridge, Cambridge, CB3 0WA, UK*
[d] *Department of Earth Sciences, University of Cambridge, Downing Street, Cambridge, CB2 3EQ, UK*
[e] *British Geological Survey, Murchison House, Edinburgh, EH9 3LA, UK*
[f] *British Geological Survey, Keyworth, Nottingham, NG12 5GG, UK*

Abstract

Numerical modeling plays an essential role in both identifying and assessing sub-surface reservoirs that might be suitable for future carbon capture and storage projects. Accuracy of flow simulations is tested by benchmarking against historic observations from on-going CO_2 injection sites. At the Sleipner project located in the North Sea, a suite of time-lapse seismic reflection surveys enables the three-dimensional distribution of CO_2 at the top of the reservoir to be determined as a function of time. Previous attempts have used Darcy flow simulators to model CO_2 migration throughout this layer, given the volume of injection with time and the location of the injection point. Due primarily to computational limitations preventing adequate exploration of model parameter space, these simulations usually fail to match the observed distribution of CO_2 as a function of space and time. To circumvent these limitations, we develop a vertically-integrated fluid flow simulator that is based upon the theory of topographically controlled, porous gravity currents. This computationally efficient scheme can be used to invert for the spatial distribution of reservoir permeability required to minimize differ-

*Corresponding Author
Email address: `j.neufeld@bpi.cam.ac.uk` ()

ences between observed and calculated CO_2 distributions. When a uniform reservoir permeability is assumed, inverse modeling is unable to adequately match migration of CO_2 at the top of the reservoir. If, however, the width and permeability of a mapped channel deposit are allowed to independently vary, a satisfactory match between observed and calculated CO_2 distributions is obtained. Finally, the ability of this algorithm to forecast the flow of CO_2 at the top of the reservoir is assessed. By dividing the complete set of seismic reflection surveys into training and validation subsets, we find that the spatial pattern of permeability required to match the training subset can successfully predict CO_2 migration for the validation subset. This ability suggests that it might be feasible to forecast migration patterns into the future with a degree of confidence. Nevertheless, our analysis highlights the difficulty in estimating reservoir parameters away from the region swept by CO_2 without additional observational constraints.

Keywords: Geologic CO_2 storage, Numerical fluid flow simulation, Porous gravity current

1. Introduction

Storage of carbon dioxide in sub-surface geologic reservoirs is generally considered to be a key component of greenhouse gas emission reduction strategies (IPCC, 2014) For safe and effective storage results, CO_2 should be stored securely in isolation from the atmosphere for thousands of years (Bickle, 2009). The largest available reservoirs occur within sedimentary rocks and consist of either depleted hydrocarbon fields or pristine saline aquifers (Bachu, 2000). Here, we concentrate on the suitability of saline aquifers for safe storage. To determine the storage security of supercritical CO_2 trapped at depth and to demonstrate conformance between observed and simulated CO_2 migration, the flow of injected CO_2 must be numerically modeled over appropriate time and length scales (Chadwick and Noy, 2015). Storage reservoirs generally have complex geometries and geologic heterogeneities that directly affect parameters such as permeability, which in turn influence fluid migration. To understand the relationship between reservoir structure and fluid flow, it is important that observations from existing storage sites are exploited to test and improve both the accuracy and reliability of numerical simulations.

At the Sleipner carbon capture and storage project in the North Sea, seven post-injection seismic reflection surveys acquired over the CO_2-filled reservoir provide insights into the migration of CO_2 through complex porous media at field scale (Figure 1a; Arts et al., 2004; Bickle et al., 2007; Boait et al., 2012). At this site, ~ 1 Mt yr^{-1} of CO_2 is injected into a pristine sandstone reservoir at a depth of 1000 m (Chadwick and Noy, 2015). Interpretation and analysis of time-lapse seismic surveys shows that CO_2 is distributed within nine discrete layers (Figure 1b). The CO_2 ponds beneath a stacked series of 1 m thick, impermeable shale horizons that are vertically distributed at about 30 m intervals through the Utsira Formation (Zweigel et al., 2004). The shale horizon immediately below the uppermost CO_2 accumulation is approximately 5 m thick and separates the uppermost section of the reservoir, known as the Sand Wedge, from the rest of the formation (Figure 1c).

The stratigraphically highest Layer 9 is of particular interest since the distribution of CO_2 within this layer is complex and there is no evidence of vertical leakage from this layer. Previously, modeling of CO_2 flow through Layer 9 has focused primarily on matching seismically observed areal planforms as a function of time (Chadwick and Noy, 2010; Cavanagh, 2013). This restriction is a consequence of the limited vertical resolution since the thickness of a thin layer is difficult to seismically image. Recently, an inverse modeling technique has been developed for determining the thickness of thin CO_2-filled layers by combining measurements of the amplitude of a reflection with small changes in two-way travel time between time-lapse surveys (Cowton et al., 2016). These authors applied this inverse method to each of the time-lapse seismic reflection surveys in order to accurately map the thickness of CO_2-saturated rock within Layer 9 as a function of time. The resultant volumetric estimates can be used to address the important goal of understanding CO_2 flow dynamics within Layer 9.

In this contribution, we develop a simple numerical reservoir simulator to model the flow of CO_2 through an unconfined porous medium beneath a complex caprock topography. By using a vertically-integrated formulation of the governing equations, this simulator is computationally efficient. A significant benefit of this efficiency is that it enables the inverse problem to be addressed: namely, what spatial distribution of permeability can best account for the flow of CO_2 within Layer 9? First, the optimal distribution of permeability is calculated using a training subset of seismic surveys. Secondly, our results are validated by exploiting a later sub-set of seismic surveys. In this way, a reliable forecasting strategy to predict the future flow of CO_2 within Layer 9 of the Sleipner reservoir is developed.

2. Previous Research

Existing approaches for modeling CO_2 migration at the Sleipner Field exploit industry-standard reservoir simulators such as GEM (Geomechanical Modeling; CMG, 2009), ECLIPSE (Exploration Consultants Limited Implicit Program for Simulation Engineering; Schlumberger, 2011), and TOUGH2 (Transport Of Unsaturated Groundwater and Heat; Pruess, 1991). These different methods solve Darcy's law for flow through porous media on a three-dimensional grid. Such sophisticated Darcy flow simulators are capable of forecasting the flow of CO_2 through complex geologic reservoirs but they are computationally expensive for two reasons. First, four-dimensional simulations have a large number of adjustable parameter values. Secondly, simulations must be carried out on length scales of kilometers and on time scales of tens to hundreds of years. As a result, coarse grid sizes are used to reduce computation time which means that significant boundary conditions, such as caprock topography, can be under-resolved (Oldenburg et al., 2016). High performance computing can be used to carry out simulations with a finer grid spacing on large domains by employing a massively parallel simulator such as PFLOTRAN (Lichtner et al., 2015). However, the use of such computing power is expensive and it is not always available or appropriate for regular use.

Matching the complex spatial distribution of CO_2 within Layer 9 and especially the rapid migration rate of CO_2 along a prominent north-striking ridge has proved a particularly difficult challenge for typical reservoir simulators. For example, the TOUGH2 software package has been used to simulate CO_2 flow in this layer with an isotropic permeability of 3 D ($\approx 3 \times 10^{-12}$ m^2). The predicted planforms are approximately radial even though the topography of the caprock is complex (Chadwick and Noy, 2010). The match between observed and calculated planforms can be improved by incorporating anisotropic permeability (i.e. 10 D and 3 D in north-south and east-west directions, respectively). Nevertheless, realistic migration rates along the north-striking topographic ridge are difficult to reproduce. Using a simpler 'black oil' simulator that ignores changes in composition, Cavanagh (2013) found that a better match between observed and calculated planforms is found by injecting the observed amount of CO_2 over the appropriate timescale, and then halting CO_2 injection into Layer 9 and running the simulation for a further ∼100 years. In this way, injection pressure is allowed to dissipate over tens of years and CO_2 spreads as a result of buoyancy alone. This predicted long-term behavior suggests that flow within Layer 9 could be driven primarily by buoyancy and not by injection pressure. One possible solution to this modeling issue is to include lower CO_2-filled layers in the numerical simulation, which removes Layer 9 from the vicinity of the injection point (Lindeberg et al., 2001). However, computational limitations mean that grid sizes would have to be dramatically increased, which would decrease the resolution for flow within Layer 9.

Zweigel et al. (2004) identified a possible high permeability channel within Layer 9. Subsequently, Williams and Chadwick (2017) used the ECLIPSE 100 simulator with a channel permeability of 8 D, and a bulk reservoir permeability of 3 D. This simulation yields a better match between the observed and calculated planforms for most of Layer 9. However, it still does not match the observed rate of migration along the ridge.

Computation time for modeling CO_2 flow on physically appropriate length scales and time scales can be significantly reduced by employing a reservoir simulator with reduced complexity (e.g. Bandilla et al., 2014; Nilsen et al., 2016). Less complex simulators exploit analytical analysis of vertically-equilibrated models and apply it to geologically realistic settings. Since these simulators use a vertically-integrated formulation, fluid flow can be solved on a two-dimensional grid which significantly increases computational efficiency. For example, Bandilla et al. (2014) report running times of several minutes on a single core for their vertically equilibrated model when simulating CO_2 flow in Layer 9 using the International Energy Agency Greenhouse Gas Research and Development Programme (IEAGHG) benchmark (50×50 m grid; Singh et al., 2010). This value compares favorably with several hours on 100 cores for a typical TOUGH2 simulation with identical input parameters. Comparative studies show that these different simulators yield broadly similar results (Nilsen et al., 2011; Bandilla et al., 2014).

Finally, Nilsen et al. (2017) exploit the adjoint method to invert for caprock topography, permeability, CO_2 density, porosity and injection rates. This method yields an excellent match to estimated thickness measurements of Layer 9 for calendar years 2001, 2004, 2006 and 2010 (Chadwick and Noy, 2010; Furre and Eiken, 2014). Their analysis shows that a generalized inverse model with many adjustable parameters can yield an accurate match to observations. However, the formulation used by Nilsen et al. (2017) yields a non-unique set of parameters that are not necessarily constrained by additional observational constraints. For example, changes in any combination of permeability, density or caprock topography can reduce CO_2 flux through a grid cell. If all parameters are allowed to vary, the likelihood of matching observations increases at the expense of insight gained. Consequently, the results of Nilsen et al. (2017) are only a partially satisfactory explanation of the spreading planform of CO_2 within Layer 9.

In summary, the problem of matching observed spreading rates for Layer 9 is not necessarily resolved by employing a new formulation of the governing equations. Nonetheless, the development of simulators with greatly reduced computational times opens up the possibility of investigating uncertainties in model space by facilitating an inverse modeling approach.

3. Modeling Strategy

The reservoir model described here simulates the flow of CO_2 through saturated porous media as a buoyancy-driven gravity current. A key feature of these currents is that their lateral extent is about one hundred times greater than their thickness. This characteristic aspect ratio is observed for all nine CO_2-filled layers at the Sleipner Field. Laboratory studies also demonstrate that flow of a density-driven invading fluid through porous media can be accurately described by a gravity current (Huppert and Woods, 1995; Golding et al., 2011). In its simplest form, the governing equation of a gravity current is vertically-integrated, which means that vertical changes in reservoir properties are incorporated as depth-averaged quantities.

A significant consideration when modeling CO_2 flow through porous media is whether the reservoir is confined or unconfined. A reservoir is unconfined if the flow of ambient water can be neglected. This assumption is valid when the thickness of the reservoir unit is much greater than the thickness of the intruding fluid. Pegler et al. (2014) found that confinement can be neglected provided that

$$h \ll \frac{\mu_c}{\mu_a} H_a, \tag{1}$$

where h is the thickness of the CO_2-saturated layer, H_a is the thickness of the reservoir unit, μ_c is the viscosity of supercritical CO_2, and μ_a is the viscosity of the ambient water.

At the Sleipner Field, the uppermost unit of the Utsira Formation that includes Layer 9 is known as the Sand Wedge (Figure 2b). The top surface of this unit is bounded by the caprock of the Utsira Formation and its base is marked by a 5 m thick shale layer. This reservoir is estimated to be $\sim$ 20 m thick, increasing to 30 m where the CO_2 layer is thickest (Williams and Chadwick, 2017). A viscosity ratio of $\mu_c/\mu_a \simeq 0.1$ implies that the CO_2 layer behaves as an unconfined current wherever it is thinner than 2–3 m— a circumstance that probably holds during the early stages of flow and at the nose of the gravity current. We note that Equation (1) is an approximation that applies to a uniform, two-dimensional reservoir and does not include the effects of topographic gradients within the caprock. This *caveat* suggests that the unconfined approximation may be used for complex three-dimensional geometries with modest confinement. Here, we make the simplifying assumption that the current is unconfined at all times and explore the ability of such a simulator to explain the observed spreading patterns.

We have chosen to neglect capillary forces that give rise to partially saturated currents. The results of centrifuge experiments carried out on core material from the Utsira Formation yield vertical CO_2 saturation profiles which suggest that the capillary transition zone at the base of the CO_2 layer is approximately 1 m thick (Chadwick et al., 2004). Other experimental and analytical results suggest that the rate of CO_2 migration is not significantly impeded by capillary forces during the injection phase (Golding et al., 2011).

Our simple model describes the flow of a single-phase gravity current with a sharp interface along a slope within an unconfined saline aquifer. Fluid flow in porous media is governed by Darcy's law,

$$\phi \tilde{u} = \mathbf{u} = -\frac{k}{\mu} \left(\nabla P + \rho g \hat{z} \right), \tag{2}$$

where ϕ is the porosity, $\tilde{u}$ is the interstitial fluid velocity, $\mathbf{u} = (u, v, w)$ is the

Darcy velocity or volumetric fluid flux, k is the permeability, μ the viscosity of CO_2, ∇P is the pressure gradient, ρ the density of the fluid, g is gravitational acceleration, and $\hat{z}$ is a unit vector in the vertical direction (Figure 3). We treat the flow of CO_2 as incompressible so that

$$\nabla \cdot \mathbf{u} = 0. \tag{3}$$

For a long, thin gravity current flowing beneath an impermeable boundary with topography $d(x, y)$, the vertical velocity is negligible and hence the pressure is hydrostatic,

$$P = \begin{cases} P_H - \rho_a g[H - (d+h)] - \rho_c g[(d+h) - z], & d < z < d+h, \\ P_H - \rho_a g(H - z), & d+h < z < H, \end{cases} \tag{4}$$

where P_H is the pressure at a reference horizon beneath the gravity current at depth $z = H$, ρ_c is the density of the injected buoyant fluid, ρ_a is the density of the ambient water, and $h(x, y, t)$ is the thickness of CO_2-saturated rock (i.e. the gravity current). In contrast to the models of Huppert and Woods (1995) and Vella and Huppert (2006) that are formulated in a slope-parallel reference frame, this model uses a horizontal reference for which it is simpler to compute complex reservoir geometries (e.g. Figure 2a).

From Darcy's law, the horizontal Darcy velocity, $\mathbf{u_H} = (u, v)$, is given by

$$\mathbf{u_H} = -\frac{k}{\mu}\nabla_H P = -\frac{kg\Delta\rho}{\mu}\nabla_H(d+h), \tag{5}$$

where ∇_H is the horizontal gradient operator, $\Delta\rho = (\rho_a - \rho_c)$ is the density difference between the two fluids , and $u_b = kg\Delta\rho/\mu$ is the buoyancy velocity.

For vertically uniform permeability, flow within the current is uniform as a function of depth. Integrating the divergence of the Darcy velocity over the depth of the current in combination with Equation 5 yields

$$\phi\frac{\partial h}{\partial t} - \nabla_H \cdot \left\{\frac{k\Delta\rho g}{\mu} h \nabla_H d\right\} = \nabla_H \cdot \left\{\frac{k\Delta\rho g}{\mu} h \nabla_H h\right\}. \tag{6}$$

This formulation highlights that the change in thickness of the CO_2 current with time is driven by advection of CO_2 caused by topographic gradients within the caprock and by diffusion of CO_2 away from regions where the gravity current is thickest.

The model described by Equation 6 is a simplified version of so-called vertical equilibrium models developed over the last decade (e.g. Golding et al., 2011; Guo et al., 2014; Andersen et al., 2015). Such models exploit the large aspect ratio of spreading currents of CO_2 to reduce the complexity of flow simulations in three dimensions by assuming that flow predominantly occurs in the horizontal, or along-slope, direction. The large aspect ratio implies that pressure is, to leading order, hydrostatic which means that flow is driven by gradients in the depth of the current and by gravity acting along slope for topographically controlled, unconfined currents. Many of these models also treat partial saturation within the CO_2 plume. Here, given both the advantageous geometry and the pore structure of the Utsira sandstone, we can confidently neglect these complicating features and focus on using this simplified approach to understand what principally controls CO_2 flow at the Sleipner Field. In this sense, The model presented here is a useful test of the efficacy of vertical equilibrium models when matching field observations.

We solve Equation (6) using a Crank-Nicholson finite difference scheme that is centered in time and space (Press et al., 2007). Subsequent time steps are solved efficiently by using tridiagonal elimination. A predictor-corrector scheme is used to evaluate non-linear diffusive buoyancy (Press et al., 2007). To improve the stability of this numerical solution in regions that are susceptible to numerical instability (e.g. sharp changes in topographic gradient), the Il'in three-point differencing scheme is applied (Il'in, 1969; Clauser and Kiesner, 1987). This scheme automatically determines the amount of 'upwinding' required to keep the model stable for high Peclet numbers. An alternating direction implicit (ADI) scheme is adapted to propagate the gravity current in three dimensions (Peaceman and Rachford, 1955; Press et al., 2007). This numerical scheme has been carefully benchmarked against analytical solutions for simplified gravity currents in both two- and three- dimensions presented by Huppert and Woods (1995) and Vella and Huppert (2006), respectively.

4. Application

Solutions of Equation (6) yield predicted distributions of CO_2, $h(x, y, t)$, that can be directly compared with the observed distribution obtained by analyzing seismic reflection surveys (Cowton et al., 2016). The geometry of the reservoir and its physical properties, for example the shape of the impermeable boundary along which CO_2 fluid is spreading, $d(x, y)$, and the permeability, $k(x, y)$, and porosity, $\phi(x, y)$, must be determined. In addition, the volumetric flux of CO_2 into Layer 9 at the top of the reservoir, $V(t)$, together with the location of the injection point are required. Finally, the density and viscosity of supercritical CO_2 must be estimated.

4.1. Reservoir Geometry and Properties

The reservoir geometry is constrained by picking the bright reflection that marks the top of the Utsira Formation on the 1994 baseline seismic reflection survey. This survey was binned into 12.5×12.5 m blocks before signal processing. The dominant frequency of the stacked seismic volume is 30 Hz which means that the vertical and horizontal resolution is about 16 m. This value limits the scale of topographic features that can be resolved. A reflection at the top of the Utsira Formation can also be easily picked on subsequent seismic surveys. Differences between two-way travel time maps of this reflection are as small as ± 1 ms which suggests that estimates of reservoir topography are robust but affected by noise of order ± 1 m (Cowton et al., 2016). To mitigate short wavelength noise, a median filter with 50 m block sizes is applied to the picked surface on each time-lapse survey (Hall, 2007). Each filtered surface is then interpolated using a continuous curvature spline with a tension factor of 0.1 (Smith and Wessel, 1990). By smoothing picked surfaces in this way, spikes, sinks and other unphysically sharp gradients that could affect the stability of numerical flow simulations are removed. The top of the Utsira Formation is not affected by faulting in the vicinity of the injection site.

The topographic surface of the caprock is picked in two-way travel time (twtt) and is converted into meters below sea-level using

$$d = \left(\frac{t_{rc}}{2}\right) V_{sed} - c, \tag{7}$$

where d is the relative depth to the reservoir-caprock boundary in meters, t_{rc} is the two-way travel time down to this boundary, $V_{sed} = 2150$ m s^{-1} is the acoustic velocity of the Nordland Shale Formation (i.e. the overlying stratigraphic unit), and $c = 115$ m is a constant obtained from sonic log measurements that enables relative depth to be synchronized to true depth (Figure 2a). Chadwick et al. (2016) report that, although there is no systematic spatial variation in stacking velocities determined during seismic processing, the uncertainty in the value of V_{sed} is ± 46 m s^{-1}. Values of V_{sed} calculated using sonic log measurements from nearby wells fall within the range of 2133–2159 m s^{-1}. Uncertainties in the regional velocity of the Nordland Shale Formation contribute to uncertainty in the magnitude of topographic gradients, whereas local variability of velocity affects the detailed pattern of topographic relief.

Pre-existing gas-rich pockets within the Nordland Formation demonstrate that the assumption of a uniform velocity within the overburden does not hold across the survey region. These pockets have lower acoustic velocities than those of the surrounding brine-saturated rock. Consequently, their presence systematically increases the calculated depth down to the reservoir-caprock boundary in these regions and disrupts the coherency of underlying reflections. In these circumstances, topographic measurements are interpolated and filled across any gaps in mapping (Smith and Wessel, 1990).

Porosity and permeability of the Utsira Formation are estimated using core material from a well located $\sim$1 km from the injection point (Zweigel et al., 2004). This formation is composed of largely unconsolidated sand grains with a bimodal grain size distribution showing peaks at 3 μm and at 0.2 mm. In core samples, its porosity is $\phi = 0.37 \pm 0.03$ which agrees with estimates from wireline logs. Measured permeabilities of the Utsira Formation are $k =$ 2–5 D (Lindeberg et al., 2001; Zweigel et al., 2004). Well tests from the nearby Grane and Oseberg areas suggest that permeability could have a bigger range of 1–8 D (Zweigel et al., 2004).

The thickness of the Sand Wedge unit is shown in Figure 2b. A pronounced linear feature that runs approximately north-south has been previously interpreted as a submarine channel deposit (Zweigel et al., 2004). Such channels are characteristic of the Utsira Formation (Gregersen, 1998). In this case, the mapped channel has a similar scale and sinuosity to low sinuosity submarine channels described elsewhere (Clark and Pickering, 1996). Sediments deposited within channels are often coarser grained as a result of faster flow velocities within the channel and are likely to have higher permeabilities (Beard and Weyl, 1973). These high permeability channels can play an significant role in fluid migration.

4.2. Fluid Properties and Injection Rates

Layer 9 sits at the top of the reservoir where the hydrostatic pressure is 8.2–8.9 MPa and temperature is 28.4–30.7 ° C (Alnes et al., 2011). These estimates are close to the critical point on the phase diagram which means that estimates of the density and viscosity of CO_2 within Layer 9 are sensitive to small changes in temperature within the saline reservoir. Alnes et al. (2011) calculated that the average density of CO_2 within the reservoir is 675 ± 20 kg m^{-3} by modeling time-lapse micro-gravity measurements. This estimate agrees with that determined by modeling the temperature history of the CO_2 plume for the entire reservoir with the PFLOTRAN software package that solves for multi-phase reactive flow and transport within a porous medium (Lichtner et al., 2015; Williams and Chadwick, 2017). Here, we use a slightly higher value of 690 ± 30 kg m^{-3} to account for cooling of CO_2 away from the injection point. Finally, the dynamic viscosity of CO_2 at pressures and temperatures that are characteristic of the top part of the reservoir is $\mu_c = 5 \pm 1 \times 10^{-5}$ Pa s (Bickle et al., 2007; Williams and Chadwick, 2017).

The existence of sub-vertical seismic chimneys described by Chadwick et al. (2004) and by Cowton et al. (2016) is consistent with vertical migration of CO_2 through the reservoir rocks. One major chimney correlates closely with the first observed accumulation of CO_2 in different layers. Therefore, it is reasonable to infer that the location of this chimney is likely to be the most significant injection point for Layer 9 (Figure 2c and Figure 4g,n). On Figure 4f, a small disconnected patch of CO_2 exists south of the significant CO_2-filled layer on the seismic survey for calendar year 2008. This outlying patch connects with the rest of the CO_2-filled distribution on the 2010 survey. Its existence suggests that there may be at least one other, albeit considerably smaller, injection point for Layer 9. For simplicity, we assume that its contribution is negligible and that most CO_2 is injected through the largest central chimney (Cowton et al., 2016).

Finally, the flux of CO_2 fluid into Layer 9 is estimated from the detailed volume calculations of Cowton et al. (2016). Re-evaluation of their calculations suggest that the volumetric injection rate is given by

$$q = \frac{dV(t)}{dt} = nC\,(t - t_0)^{n-1}\,, \tag{8}$$

where $C = 9500 \pm 5700$ m^3 yr^{-n}, $t_0 = 1998.1 \pm 0.5$ and $n = 2.1 \pm 0.2$. The uncertainty of this injection rate is estimated from CO_2 thickness measurements which includes the uncertainty of the acoustic velocity of CO_2-saturated sandstone (Cowton et al., 2016).

5. Results of Inverse Modeling

By adopting a vertically-integrated formulation, the flow model presented here is considerably more efficient than conventional Darcy flow simulators. Each of our simulations takes less than ∼10 minutes to run on a single core. This short calculation time means that the best-fitting value of permeability that minimizes the difference between the observed and calculated CO_2 distributions can be determined by inverse modeling. At each stage, a starting model is computed using permeability values measured from nearby boreholes. The influence of uniform and spatially variable permeabilities is investigated by grid search.

Simulated CO_2 flow throughout Layer 9 for a uniform permeability of $k = 2$ D is compared with the observed CO_2 distribution (Figure 4a-g, o-u; Cowton et al., 2016). In this simulation, it is clear that the northerly extension of the plume along the topographic ridge at the top of the reservoir does not move rapidly enough to reach the northern topographic dome. Instead, the sluggish spreading rate causes CO_2 to accumulate adjacent to the injection point where it reaches a thickness of 12 m by 2010 which is considerably greater than observed.

The principal result of constant permeability simulations is that using different combinations of input parameters does not yield adequate matches between observed and calculated CO_2 distributions. For example, uncertainties in the detailed shape of caprock topography could potentially account for significant discrepancies (Chadwick et al., 2016). However, to significantly improve the match between observed and calculated planforms at the northern end of survey, the topographic gradient would need to be increased by as much as 50 m. This value is substantially greater than permitted by uncertainties in the acoustic velocity of the Nordland Shale Formation. Alternatively, the physical properties of supercritical CO_2 may vary within Layer 9 since the estimated pressure and temperature are close to the critical point. Changes in these properties directly affect the value of the buoyancy velocity, u_b. Here, we note that quoted uncertainties in $\Delta\rho$ and μ for $k = 2$ D yields $u_b = 1.4^{+0.5}_{-0.3} \times 10^{-4}$ m s^{-1}. This range is equivalent to changes in permeability of $k = 2^{+0.7}_{-0.5}$ D.

5.1. Uniform Permeability

The mismatch between observed and simulated CO_2 distributions is substantial, which suggest that the assumption of a uniform permeability of $k = 2$ D is incorrect notwithstanding uncertainties in the fluid properties injected CO_2 fluid within Layer 9. Here, we first explore simulations where different but constant values of k are assumed. A parameter sweep is performed to find the optimal permeability for Layer 9. For each value of k, the calculated distribution of CO_2 is compared with the observed distribution using a misfit function

$$M = \frac{1}{N_s} \sum_{j=1999}^{N_s} \left[\frac{1}{N} \sum_{i=1}^{N} \left(\frac{h^c_{ij} - h^o_{ij}}{\sigma_{ij}} \right)^2 \right]^{1/2}, \tag{9}$$

where h^c_{ij} is the calculated thickness of the CO_2 layer, h^o_{ij} is the observed thickness, and σ_{ij} is the standard deviation of the observed thickness (Figure 5a; Cowton et al., 2016). Here, i refers to a particular thickness value out of a total of N values from each survey where the observed CO_2-filled layer is > 0.5 m thick, and j refers to a given seismic reflection survey between calendar years 1999 and 2010 where N_s is the total number of surveys.

Our estimates of standard deviation are deliberately conservative. Thus for $h^o_{ij} > 5$ m, σ is determined from synthetic tests but for $h^o_{ij} < 5$ m we apply a large uniform uncertainty of $\sigma = 0.5$ m. This uniform uncertainty account for errors in caprock topography that can cause discrepancies between observed and calculated CO_2 thicknesses, particularly in regions where Layer 9 is very thin. A threshold of 0.5 m is chosen based on the uncertainty in reliably resolving the thickness of a thin layer on a seismic reflection survey with a given frequency content (Figure 5a).

A parameter sweep of k shows that a broad global minimum of residual misfit between observed and calculated CO_2 thicknesses occurs for k = 5–12 D (Figure 5b). Despite this success, the spatial distribution of CO_2 and its observed rate of northward migration cannot be matched, even when k = 12 D (Figure 4h-n and o-u). At the southern end of the planform, there is also significant misfit between observed and calculated distributions. Therefore although high values of permeability can generally account for a rapid rate toward the north, the southward spread of CO_2 requires a lower permeability to allow ponding of CO_2 close to the injection point. These remaining discrepancies suggest that a more complex spatial pattern of permeability is required.

5.2. Spatially Variable Permeability

Our justification for investigating the consequences of a more complex pattern of permeability is centered on the existence of a notable, 25–30 m thick, linear channel that curves and splays northward (Figure 2b). A series of small crevasse splays can be interpreted along the left-hand bank of this feature which suggests that it is a channelized submarine fan deposit. It is well known that these channel deposits can have high values of porosity and permeability which make them favorable hydrocarbon exploration targets. Eldrett et al. (2015) observe that in the Paleocene Sele Formation, North Sea, the permeability contrast between high-quality sands deposited within channels and the overbank and levee facies is typically several orders of magnitude.

Here, we test the influence that this linear permeability feature has upon flow prediction by using a simple parametrization of spatially varying permeability (Figure 2b). The region under consideration is divided into two parts comprising the linear channel and the rest of the reservoir by using three independent parameters: w, the width of the channel; k_1, the permeability of the reservoir; and k_2, the permeability of the channel (Figure 2c). Our goal is to minimize the misfit between the observed and calculated distributions of CO_2 by varying these three parameters using a simple grid search.

Figure 6 shows how misfit varies as a function of w, k_1 and k_2. A shallow global minimum occurs at $w = 700 \pm 125$ m, $k_1 = 3.5 \pm 1$ D, and $k_2 = 20 \pm 8$ D. The shape of this misfit function makes calculating formal uncertainties challenging. Our quoted uncertainties are estimated from that misfit contour which shows a 1 % increase above the global minimum. These uncertainties clearly show that k_1 is well constrained with a value that is satisfyingly close to that estimated independently from reservoir core material (Zweigel et al., 2004). There is little trade-off between k_1 and the other two parameters. The values of k_2 and w are less well constrained and exhibit the expected degree of negative trade-off (i.e. a narrower channel with a higher permeability yields as good a fit as a wider channel with lower permeability).

The optimal permeability of this channel is regarded as physically plausible when compared to experimental permeability measurements carried out on unconsolidated sand (Beard and Weyl, 1973). An empirical relationship between permeability and porosity based on measurements from the clean and well sorted Fontainebleau sandstone shows that $k \simeq 3.03 \times 10^{-4}(\phi)^{3.05}$, which suggests that rocks with a porosity of $\phi = 0.37$ can have a permeability as great as $\sim$20 D (Bourbie and Zinszner, 1985). Similarly clear correlations between porosity and permeability are also observed for Paleocene North Sea hydrocarbon reservoirs, such as the Ormen Lange field, the Maureen formation, and the Forties Sandstone member. In each case, permeabilities of $\sim$20 D are reasonable for sandstones with $\phi = 0.37$ (Grecula et al., 2015; Kilhams et al., 2015; Jones et al., 2015). These estimates are in line with a permeability calculated using the Carman-Kozeny relationship for clean sand with a mean grain size of 200 μm. Figure 7 confirms that, in order to accurately match the observed rate of migration along the length of the channel, a permeability of up to 30 D is required. We note that the predicted buoyancy velocity within this channel is too great to have been generated by reasonable variations in the density and viscosity of CO_2.

Figure 8h-n shows that the combination of lower permeability near the injection point and higher permeability within the channel provides the required heterogeneity of reservoir properties to yield an improved match to both the southward and northward migration of fluid. The largest residual misfit occurs along the eastern side where migration of CO_2 into part of the north-running ridge occurs much earlier than observed on the seismic reflection surveys. One possible explanation is that a low permeability region exists between two distinct and parallel channels, reducing the flux of CO_2 into the eastern channel. Alternatively, the topographic smoothing applied to mitigate the effects of noise may have reduced the spill-point depth in this area.

The results of running flow simulations that include spatially variable permeability suggest that vertical equilibrium algorithms can be exploited in combination with seismically derived observations to build reservoir models that predict good matches between observed and calculated CO_2 distributions throughout Layer 9. Here, we have been able to match observed migration rates by considering buoyancy driven flow with reasonable values of permeability without requiring significant changes to the observed caprock topography. Note, however, that the impact that reservoir confinement might have upon flow of CO_2 cannot be assessed using this model alone. We conclude that an inverse modeling approach can shed useful light on the properties of Layer 9 and have a role to play alongside traditional reservoir characterization techniques to improve forecasts of CO_2 flow at other potential carbon capture and storage sites.

6. Benchmarking, Testing, and Forecasting

The computational efficiency of our algorithm relies on the assumption that the flow of CO_2 may be treated as an unconfined, porous gravity current. It is important to test the results of using a vertically-integrated approach with more conventional three-dimensional flow simulators. Here, CO_2 flow within Layer 9 was also simulated by running the ECLIPSE 100 black oil reservoir model with our optimal, spatially variable, permeability distribution (Figure 8o-u). Due to the necessarily greater computation time, grid cells for the ECLIPSE 100 simulation were chosen to be twice the size of those for the vertically-integrated model (i.e. 25×25 m). These grid cells were vertically spaced 1 m apart and the reservoir was assumed to be 24 m thick with an impermeable lower boundary. Other parameters such as caprock topography, reservoir properties, rate of injection, locus of injection point, and fluid properties are unchanged.

The results of the ECLIPSE 100 simulation are nearly identical to those of our vertically-integrated model (compare Figure 8o-u and h-n). Inclusion of an impermeable lower boundary condition does not appear to make a significant difference, which strongly supports our assumption of an unconfined reservoir. Minor differences can probably be attributed to the reduced resolution of caprock topography used in the ECLIPSE 100 simulation (Figure 8v-ab). Note that this simulation took approximately one hundred times longer to run than the vertically-integrated model on a single core. This substantial difference in computation time confirms that an inverse permeability model based upon conventional flow simulators is, at present, impractical. It is also worth noting that, within the constraints of the gravity current approximation, improved horizontal is achieved with the vertically-integrated simulations.

A reservoir simulator should have the ability to forecast future flow through a given reservoir model. To test the ability of our vertically averaged simulator to predict CO_2 flow at the Sleipner Field, we have divided the set of time-lapse seismic images from surveys for all seven calendar years into different training and validation sub-sets (Table 1). In each case, the training sub-set of surveys are used to identify optimal reservoir parameters by minimizing the misfit between observed and calculated flow distributions (Equation 9). These results are then used to predict flow distributions for the validation sub-set. Confidence in the simulator depends upon its ability to independently predict flow distributions that have a small residual misfit compared with the baseline performance that is calculated using the entire set. We acknowledge that this machine-learning approach is less useful when the number of sets of observations is small. However, the significant expense of acquiring additional seismic reflection surveys suggests that testing even a limited ability to predict future behavior is a worthwhile endeavor.

Our analysis indicates that a reasonable prediction of the distribution of CO_2 up to 2008 can be made by using simulations up to and including 2004, provided that the rate of injection into Layer 9 is known (Table 1). However, our ability to predict the distribution of CO_2 for 2010 by fitting the training set shows a marked deterioration. This deterioration may be caused by a notable reduction in observed migration velocity along the northern protuberance, which suggests that permeability may decrease northward along the channel (Figure 7). This inference is in accordance with observations made by (Clark and Pickering, 1996), who suggested that deposition of sands within a channel can be variable along the length of a channel, particularly near channel bends, and cause permeability to spatially vary. An alternative possibility is that uncertainties in the detailed topography of the northern dome

Table 1: Forecasting CO_2 flow in Layer 9. Best-fitting parameters for flow model found by grid search for training set. Misfit for each seismic reflection survey for each set of trained parameters are shown in black. Misfits for test data shown in red.

Training Set	Model Parameters			Misfit						
	w, m	k_1, D	k_2, D	1999	2001	2002	2004	2006	2008	2010
1999-2010	700	3.5	20	2.88	2.21	2.31	2.60	2.86	3.35	3.33
1999-2008	650	3.5	30	2.89	2.15	2.27	2.66	2.93	3.23	3.66
1999-2006	700	3.5	20	2.88	2.21	2.31	2.60	2.86	3.35	3.33
1999-2004	650	4	28	2.88	2.17	2.28	2.62	2.95	3.26	3.63
1999-2002	650	3.5	50	2.88	2.13	2.24	2.80	3.10	3.43	4.26

give rise to discrepancies between observed and calculated distributions of CO_2.

Since supercritical CO_2 fluid is being injected into the Utsira Formation as of 2017, it is worthwhile attempting to use our vertically-integrated simulator to forecast future distributions. Here, we explore two end-member sets of forecasts that are based upon having fitted CO_2 distributions up to and including 2010. The first set assumes that no additional CO_2 is injected into Layer 9 after 2010 (Figure 9a; c-h). With zero additional flux, the distribution of CO_2 shows little further change which suggests that fluid has already reached a state of buoyant equilibrium by previously migrating rapidly from the southern to the northern dome. The second set assumes that the injection rate continues to increase in accordance with Equation 8 after 2010 (Figure 9b; i-n). In this case, the areal planform continues to increase almost linearly. Note that the volume of CO_2 trapped beneath the southern dome does not significantly increase between 2010 and 2022 and the maximum thickness only increases by ~ 3 m. The bulk of CO_2 that enters Layer 9 during this period is accounted for by an increase in the amount that is trapped beneath the northern dome. This northern dome has a significantly greater trapping capacity than the southern dome, which implies that CO_2 will continue to safely migrate into it for many years. However, as the layer of accumulated CO_2 thickens, it is likely that reservoir confinement and the consequent flow of ambient fluid will begin to influence flow dynamics. At that stage, our simplified reservoir simulator will not longer be capable of accurately describing the distribution of CO_2.

7. Discussion and Conclusions

We describe and apply a simplified numerical reservoir simulator based on buoyancy-driven gravity currents to model CO_2 flow through an unconfined porous reservoir. The vertically-integrated nature of the governing equations means that this model is computationally efficient compared to industry-standard, three-dimensional Darcy flow simulators. This reservoir simulator is used to investigate flow of CO_2 together with the reservoir properties required to reproduce the seismically-derived distribution of CO_2 in three dimensions for Layer 9 of the Sleipner Field. Flow simulations performed using measured reservoir geometry and reservoir and fluid properties only partially match the observed CO_2 distributions. Analysis of the baseline seismic reflection survey suggests the existence of a submarine channel deposit within the reservoir. A simple spatially varying reservoir model with a high permeability channel is found to reduce the misfit between observed and calculated CO_2 distributions. Consideration of the confinement of the reservoir does not appear to be required the evolution of Layer 9. Using this best-fitting reservoir model, the future flow of CO_2 within Layer 9 can be forecast by making simplified assumptions about the future flux of CO_2 into Layer 9.

An inverse modeling strategy is used to identify a reservoir permeability that permits a good match between the observed and calculated migration of CO_2 through Layer 9 of the Utsira Formation reservoir. Our comparisons and tests validate the utility of using vertically equilibrated models as the basis of inverse tools with which to assess reservoir properties. However, it is clear that there are regions in which discrepancies between observed and calculated CO_2 distributions remain. These discrepancies can be attributed to uncertainties in geologic parameters that are not permitted to vary in our inversion scheme, such as detailed caprock topography and intra-channel permeability. The high bias and low variance input permeability model used here is likely to underfit the observed CO_2 distribution (Geman et al., 1992). Equally, a low bias and high variance approach that manipulates parameters such as permeability and caprock topography on the grid square level to yield a precise match with the observed CO_2 distribution will overfit the data. The choice of parameters that would permit this match is non-unique, a problem exacerbated by the limited number of time-lapse seismic surveys and by the uncertainty in the observed CO_2 distribution.

In order to build an improved forecasting strategy, a permeability model with intermediate complexity is required. For example, our simple channel model can be made more complex by the addition of a variable permeability within the channel. However, for unconfined flows, the observed pattern of migration is only sensitive to the area swept out by the CO_2 plume. Estimating parameters in this way, outside of the swept region, is difficult without evidence from additional sources. While a generalized model could be inverted to find a more complex permeability structure this is, at present, unlikely to lead to significant improvements in the inferred reservoir model and its associated ability to forecast future CO_2 flow.

The success of this reservoir simulation, in conjunction with analysis by Bandilla et al. (2014) and Nilsen et al. (2017) amongst others, shows that vertically-integrated models are a computationally efficient alternative to conventional Darcy flow simulators when modeling the flow of CO_2 on appropriate length and time scales. These efficient models can help to improve the match between reservoir simulations and geophysical observations. Whilst limited agreement has already been demonstrated at the Ketzin site in Germany and at the Snøhvit site in Norway, the use of low-computational cost reservoir simulations to test suites of reservoir models could enhance our understanding of the sub-surface reservoir characteristics of other fields where CO_2 injection has been carried out (Grude et al., 2014; Lüth et al., 2015). A large body of literature that has already documented analytical solutions for gravity currents in different situations means that the simulator described here can be adapted quickly and easily to model CO_2 flow within other storage geologic reservoirs.

Acknowledgments

We thank the Sleipner License Partners (Statoil, Total E&P Norge and ExxonMobil) for access to seismic reflection surveys and for permission to publish our results. LRC is partly funded by the EU PANACEA and TRUST consortia. JAN acknowledges support from a Royal Society University Research Fellowship. GAW, JCW and RAC worked with support of the Norwegian CCS Research centre (NCCS) under the auspices of the Norwegian research program Centres for Environment-friendly Energy Research (FME) and publish with permission of the Executive Director, British Geological Survey (NERC). Seismic reflection surveys used in this study are listed in the references and are available on request from the Sleipner License Partners. Department of Earth Sciences Contribution Number esc.4128.

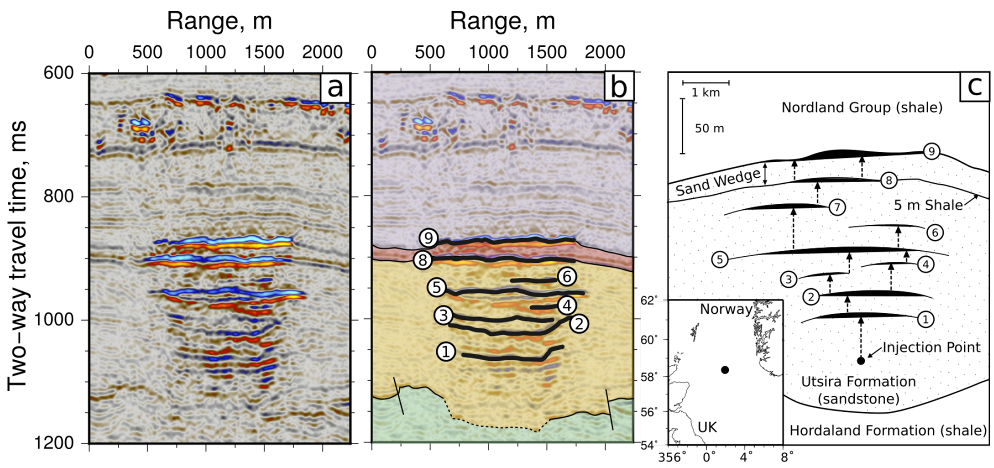

Figure 1: **(a)** Cross-line (i.e. vertical slice) from 2010 seismic reflection survey. Red/blue = positive/negative amplitude reflections. **(b)** Geologic interpretation. Numbered black layers = mappable reflections from CO_2-filled sandstone horizons; orange layer = Sand Wedge unit; yellow layer = Utsira Formation; green layer = Hordaland Formation (solid/dashed line = mappable/extrapolated top of this formation); sub-vertical lines = minor normal faults. **(c)** Schematic cross-section showing configuration of CO_2-filled horizons within saline reservoir (note vertical exaggeration). Dotted pattern = Utsira Formation; numbered black layers = nine CO_2-filled sandstone horizons separated by thin mudstones; solid circle = locus of injection well; dashed vertical arrows = putative flow of CO_2 between sandstone layers. Inset map shows general location of carbon capture and storage project at Sleipner Field.

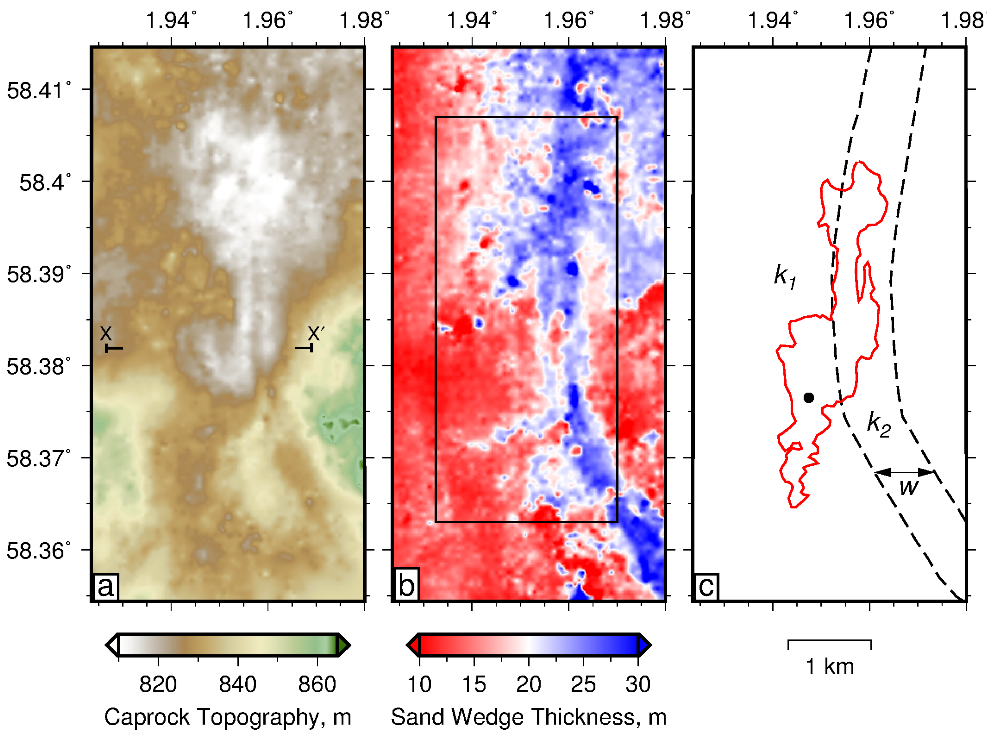

Figure 2: **(a)** Topography of upper surface of Utsira Formation (meters below sea level). X–$X\prime$ indicates location of seismic profile shown in Figure 1a-b. **(b)** Thickness of Sand Wedge unit. Solid black box = extent of modeled domain described in text. **(c)** Sketch of idealized model used for flow simulations. Solid circle = locus of CO_2 input; red line = outline of CO_2-filled Layer 9 for year 2010; pair of dashed lines = locus of putative sedimentary channel where w is width of channel in x direction, k_2 is permeability of channel, and k_1 is background permeability.

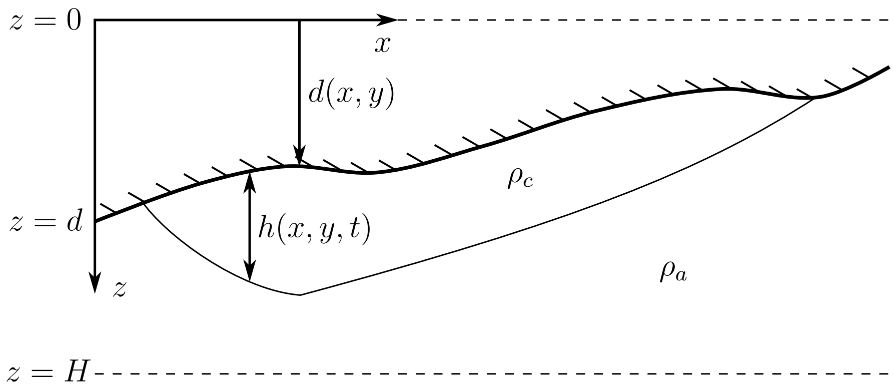

Figure 3: Sketch showing a three-dimensional geometry of gravity current along the sloping interface. Thick line with hatching = caprock interface; thin line = base of gravity current; symbols described in text.

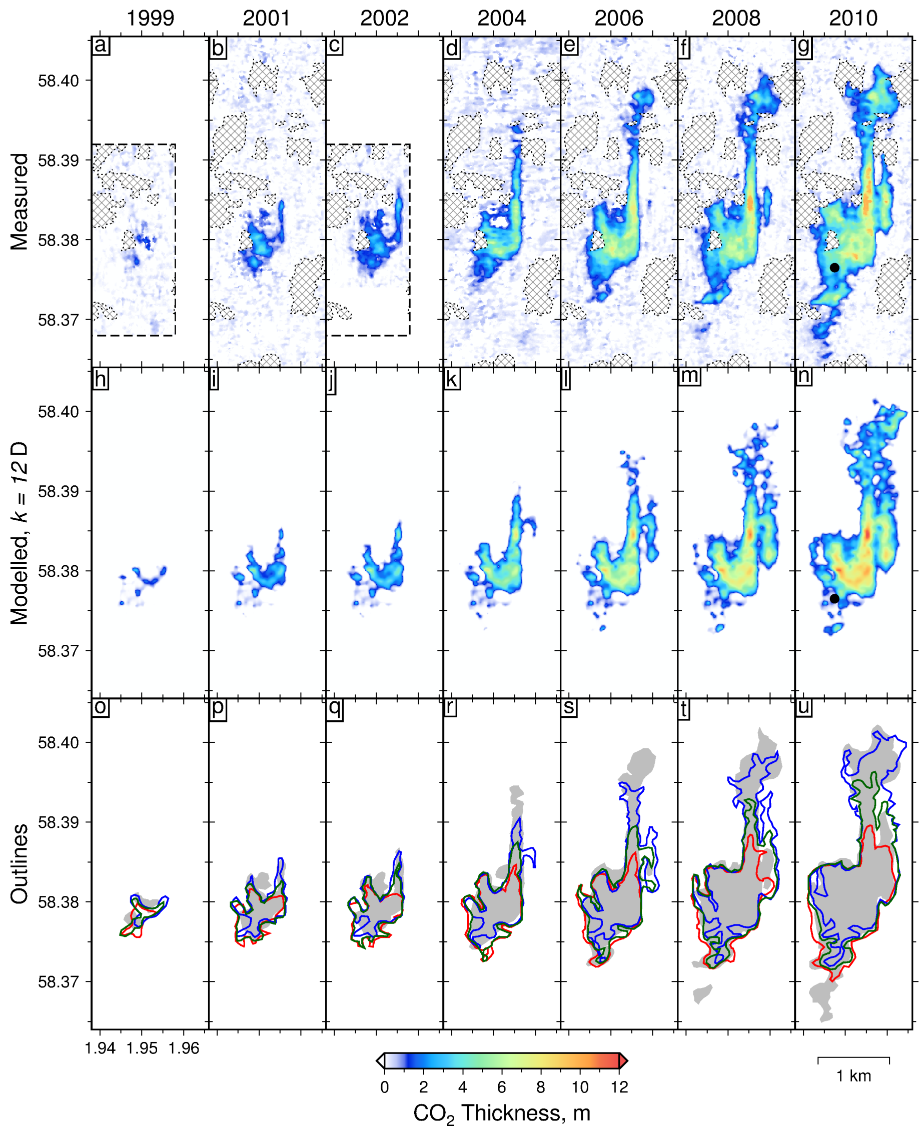

Figure 4: **(a)-(g)** Temporal sequence showing measured distributions of CO_2 thickness for years 1999–2010 determined from analysis of seismic reflection datasets (Cowton et al., 2016). Cross-hatched polygons = regions where reflections are incoherent due to pockets of natural gas within sedimentary overburden; solid circle in panel **(g)** indicates locus of inferred CO_2 input for 2010. **(h)-(n)** Temporal sequence showing predicted distributions of CO_2 thickness using k = 12 D. Solid circle as before. **(o)-(u)** Gray polygons = temporal sequence of measured distributions from panels **(a)-(g)**; polygons outlined in red/green/blue = temporal sequence of predicted distributions for k = 2, 5 and 12 D, respectively.

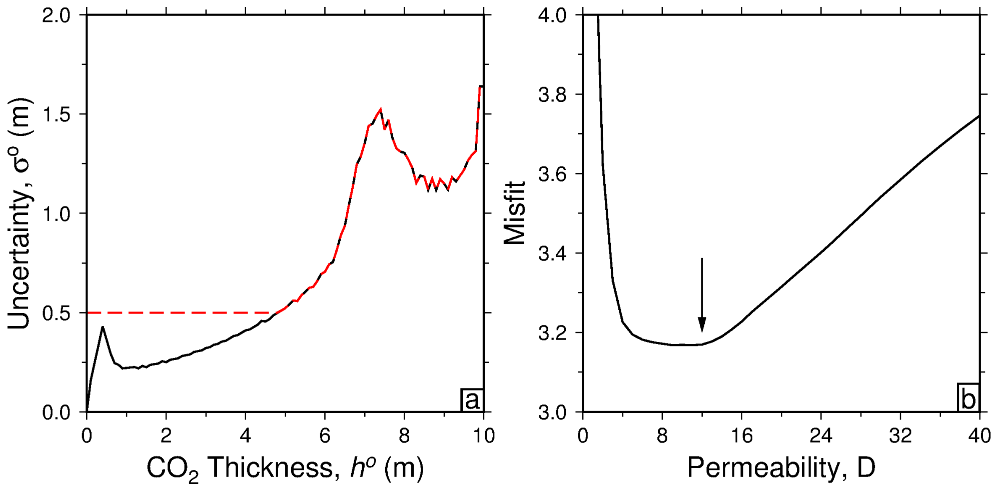

Figure 5: **(a)** Uncertainty of observed thickness measurement, σ^o, obtained using method of Cowton et al. (2016), as function of observed CO_2 thickness, h^o. Black line = values of σ^o gauged from synthetic modeling of CO_2 thickness (Cowton et al., 2016). Red dashed line = relationship between uncertainty and thickness used here for minimizing misfit function which ensures that uncertainty values for $h^o < 5$ are not unrealistically small but set as $\sigma^o = 0.5$. **(b)** Misfit as function of permeability for simulations that assume uniform permeability. Vertical arrow = position of global minimum at 12 D (see Figure 4o-u for end-members).

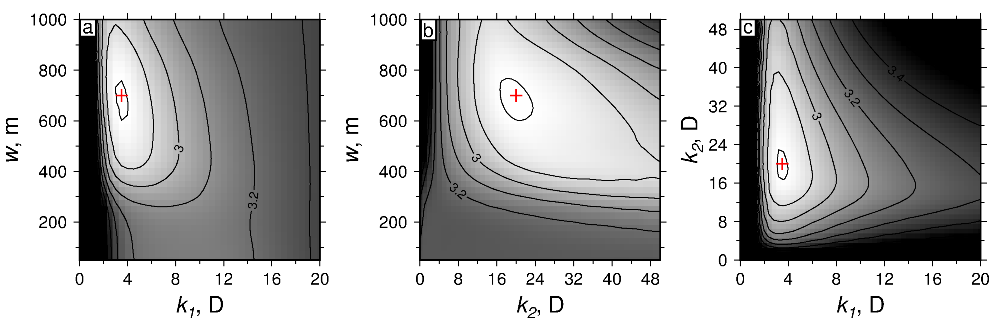

Figure 6: Orthogonal slices through w-k_1-k_2 misfit function for channel permeability model. **(a)** w-k_1 slice at k_2 = 20 D. Red cross= locus of global minimum. **(b)** w-k_2 slice at $k_1 = 3.5$ D. **(c)** k_2-k_1 slice at $w = 700$ m.

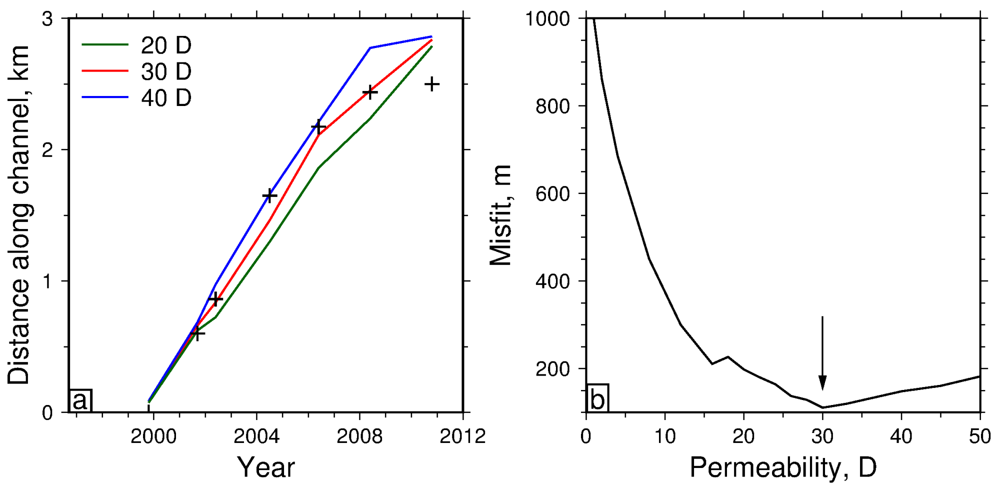

Figure 7: **(a)** Migration distance of CO_2 along channel as function of calendar year for different values of permeability. In each case, distance from estimated entry point is chosen using northernmost grid square where CO_2 thickness is greater than 0.5 m. Crosses = observed migration distances along channel for each calendar year. Green/red/blue lines = simulated migration distances as function of calendar year for k_2=20 D, 30 D and 40 D, respectively (in each case, k_1=3.5 D and w=700 m). **(b)** Misfit between observed and simulated migration rates for all calendar years as function of permeability. Vertical arrow = locus of global minimum at $k_2 = 30$ D.

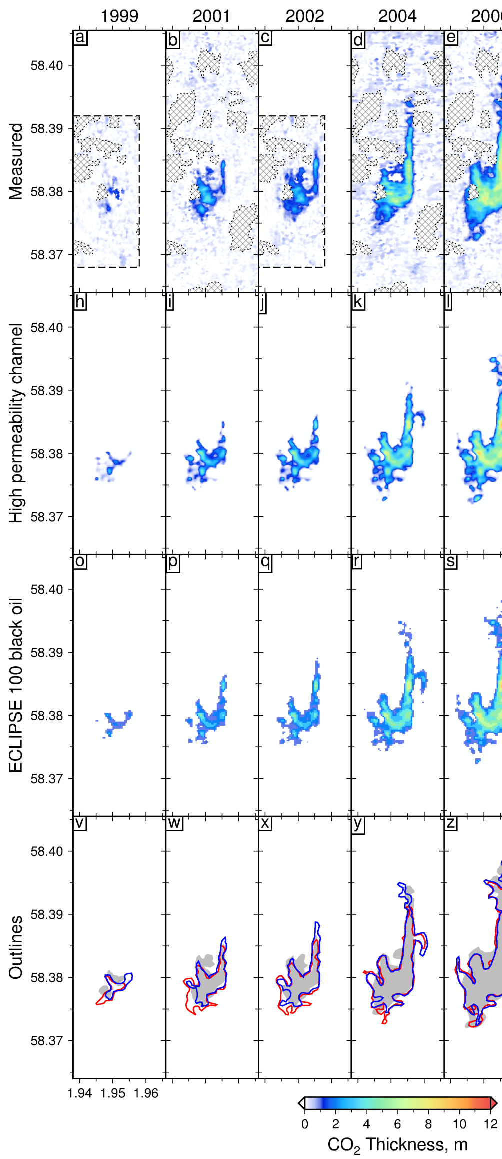

Figure 8: **(a)-(g)** Temporal sequence showing measured distributions of CO_2 thickness for years 1999–2010 determined from analysis of seismic reflection datasets (Cowton et al., 2016). Cross-hatched polygons = regions where reflections are incoherent due to pockets of natural gas within sedimentary overburden. **(h)-(n)** Temporal sequence showing distributions calculated by inverting for optimal channel permeability model where $k_1 = 3.5$ D, $k_2 = 20$ D and $w = 700$ m ($u_1 = 6.5 \times 10^{-4}$ ms^{-1}, $u_2 = 3.7 \times 10^{-3}$ ms^{-1}). **(o)-(u)** Temporal sequence showing distributions calculated using ECLIPSE 100 black oil reservoir model for identical permeability model with half the grid resolution. **(v)-(ab)** Gray polygons = temporal sequence showing measured distributions from panels **(a)-(g)**; polygons outlined in red/blue = temporal sequence of predicted distributions for vertically-integrated and ECLIPSE models, respectively.

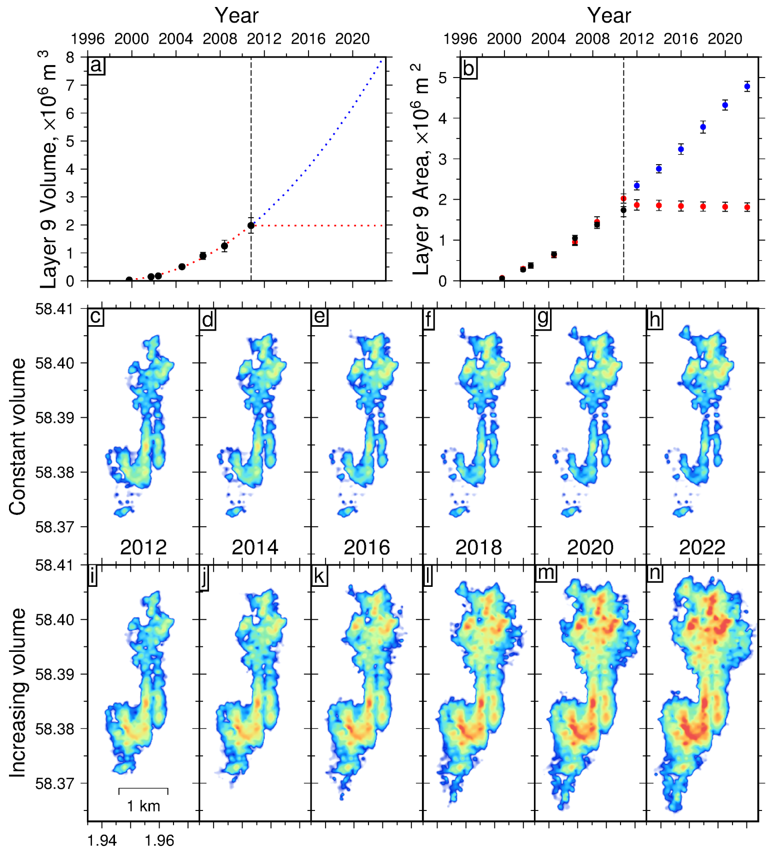

Figure 9: Forecasting calculations. **(a)** Volume of CO_2 injected into Layer 9 as function of calendar year. Solid circles = measured volumes (Cowton et al., 2016); dashed line = calendar limit of available seismic reflection surveys; red dotted line = constant volume of injection into Layer 9 at future times; blue dotted line = increasing volume of injection into Layer 9 in accordance with pre-2010 rate of injection. **(b)** Planform area of Layer 9 as function of calendar year. Solid circles = observed areas of Layer 9 measured using available seismic reflection surveys; dashed line as before; red circles = predicted areas assuming constant volume of injection; blue circles = predicted areas increasing volume of injection in accordance with pre-2010 values. **(c)-(h)** Temporal sequence showing predicted distributions of CO_2 thickness for years 2012–2022 where post-2010 injected volume remains constant. Forecasts were calculated using 700 m-wide channel with permeability of 20 D embedded in background permeability of 3.5 D. **(i)-(n)** Temporal sequence showing predicted distributions where injected volume grows in accordance with pre-2010 estimated. Color scale as for Figure 8.

Alnes, H., Eiken, O., Nooner, S., Sasagawa, G., Stenvold, T., Zumberge, M., 2011. Results from Sleipner gravity monitoring: Updated density and temperature distribution of the CO_2 plume. Energy Procedia 4, 5504–5511. URL http://dx.doi.org/10.1016/j.egypro.2011.02.536

Andersen, O., Gasda, S. E., Nilsen, H. M., 2015. Vertically averaged equations with variable density for CO_2 flow in porous media. Transport in Porous Media 107 (1), 95–127. URL https://doi.org/10.1007/s11242-014-0427-z

Arts, R., Eiken, O., Chadwick, A., Zweigel, P., van der Meer, L., Zinszner, B., 2004. Monitoring of CO_2 injected at Sleipner using time-lapse seismic data. Energy 29 (9-10), 1383–1392. URL http://www.sciencedirect.com/science/article/pii/S0360544204001550

Bachu, S., 2000. Sequestration of CO_2 in geological media: criteria and approach for site selection in response to climate change. Energy conversion and management 41 (9), 953–970. URL https://doi.org/10.1016/S0196-8904(99)00149-1

Bandilla, K. W., Celia, M. A., Leister, E., 2014. Impact of Model Complexity on CO_2 plume modeling at Sleipner. Energy Procedia 63, 3405–3415. URL http://linkinghub.elsevier.com/retrieve/pii/S1876610214021845

Beard, D., Weyl, P., 1973. Influence of texture on porosity and permeability of unconsolidated sand. Am. Assoc. Pet. Geol. Bull. 57 (2), 349–369.

Bickle, M., Chadwick, A., Huppert, H. E., Hallworth, M., Lyle, S., 2007. Modelling carbon dioxide accumulation at Sleipner: Implications for underground carbon storage. Earth Planet. Sci. Lett. 255 (1-2), 164–176. URL http://www.sciencedirect.com/science/article/pii/S0012821X06008892

Bickle, M. J., 2009. Geological carbon storage. Nat. Geosci. 2 (12), 815–818. URL http://www.nature.com/doifinder/10.1038/ngeo687

Boait, F. C., White, N. J., Bickle, M. J., Chadwick, R. A., Neufeld, J. A., Huppert, H. E., 2012. Spatial and temporal evolution of injected CO_2 at the Sleipner Field, North Sea. J. Geophys. Res. Solid Earth 117 (B3). URL http://doi.wiley.com/10.1029/2011JB008603

Bourbie, T., Zinszner, B., 1985. Hydraulic and acoustic properties as a function of porosity in Fontainebleau sandstone. J. Geophys. Res. Solid Earth 90 (B13), 11524–11532.
URL http://dx.doi.org/10.1029/JB090iB13p11524

Cavanagh, A., 2013. Benchmark Calibration and Prediction of the Sleipner CO_2 Plume from 2006 to 2012. Energy Procedia 37, 3529–3545.
URL http://www.sciencedirect.com/science/article/pii/S187661021300489X

Chadwick, R., Arts, R., Eiken, O., Kirby, G., Lindeberg, E., Zweigel, P., 2004. 4D seismic imaging of an injected $C0_2$ plume at the Sleipner Field, central North Sea. Geol. Soc. London, Mem. 29 (1), 311–320.
URL http://mem.lyellcollection.org/content/29/1/311.abstract

Chadwick, R., Noy, D., 2010. History-matching flow simulations and time-lapse seismic data from the Sleipner CO_2 plume. Geol. Soc., London, Pet. Geol. Conf. 7 (1), 1171–1182.
URL https://doi.org/10.1144/0071171

Chadwick, R., Williams, G., White, J., 2016. High-resolution imaging and characterization of a CO_2 layer at the Sleipner CO_2 storage operation, North Sea using time-lapse seismics. First Break 34 (February), 79–88.
URL http://fb.eage.org/publication/content?id=83911

Chadwick, R. A., Noy, D. J., 2015. Underground CO_2 storage: demonstrating regulatory conformance by convergence of history-matched modeled and observed CO_2 plume behavior using Sleipner time-lapse seismics. Greenh. Gases Sci. Technol. 5 (3), 305–322.
URL http://dx.doi.org/10.1002/ghg.1488

Clark, J., Pickering, K., 1996. Architectural elements and growth patterns of submarine channels: application to hydrocarbon exploration. Am. Assoc. Pet. Geol. Bull. 80 (2), 194–220.

Clauser, C., Kiesner, S., 1987. A conservative, unconditionally stable, second-order three-point differencing scheme for the diffusion-convection equation. Geophys. J. Int. 91 (3), 557–568.
URL http://gji.oxfordjournals.org/cgi/doi/10.1111/j.1365-246X.1987.tb01658.x

CMG, 2009. User's guide GEM. Tech. rep., Computer Modelling Group Ltd.
URL https://www.cmgl.ca/gem

Cowton, L. R., Neufeld, J. A., White, N. J., Bickle, M. J., White, J. C., Chadwick, R. A., 2016. An inverse method for estimating thickness and volume with time of a thin CO_2-filled layer at the Sleipner Field, North Sea. J. Geophys. Res. Solid Earth 121 (7), 5068–5085.
URL http://doi.wiley.com/10.1002/2016JB012895

Eldrett, J., Tripsanas, E., Davis, C., McKie, T., Vieira, M., Osterloff, P., Sandison, T., 2015. Sedimentological evolution of Sele Formation deep-marine depositional systems of the Central North Sea. Geological Society, London, Special Publications 403 (1), 63–98.
URL https://doi.org/10.1144/SP403.9

Furre, A. K., Eiken, O., 2014. Dual sensor streamer technology used in Sleipner CO_2 injection monitoring. Geophys. Prospect. 62 (5), 1075–1088.
URL http://dx.doi.org/10.1111/1365-2478.12120

Geman, S., Bienenstock, E., Doursat, R., 1992. Neural networks and the bias/variance dilemma. Neural Computation 4 (1), 1–58.
URL https://doi.org/10.1162/neco.1992.4.1.1

Golding, M., Neufeld, J., Hesse, M., Huppert, H., 2011. Two-phase gravity currents in porous media. J. Fluid Mech. 678, 248–270.
URL http://journals.cambridge.org/abstract_S0022112011001108

Grecula, M., Hognestad, J., Price, S., Ferrero, M. B., De Bruijn, G., Noraberg, K., Engenes, K., Mears, P., Van Ojik, K., McGarva, R., 2015. Interplay of fan-fringe reservoir deterioration and hydrodynamic aquifer: understanding the margins of gas development in the Ormen Lange Field. Geol. Soc., Lond., Spec.l Pubs. 403 (1), 157–183.
URL https://doi.org/10.1144/SP403.7

Gregersen, U., 1998. Upper Cenozoic channels and fans on 3D seismic data in the northern Norwegian North Sea. Pet. Geosci. 4 (1).
URL http://pg.geoscienceworld.org/content/4/1/67

Grude, S., Landrø, M., White, J., Torsæter, O., 2014. CO_2 saturation and thickness predictions in the Tubåen Fm., Snøhvit field, from analytical solution and time-lapse seismic data. Int. J. Greenh. Gas Control 29, 248–255.
URL https://doi.org/10.1016/j.ijggc.2015.08.005

Guo, B., Bandilla, K. W., Doster, F., Keilegavlen, E., Celia, M. A., 2014. A vertically integrated model with vertical dynamics for CO_2 storage. Water Resour. Res. 50 (8), 6269–6284.

Hall, M., 2007. Smooth operator: Smoothing seismic interpretations and attributes. Lead. Edge 26 (1), 16–20.
URL https://doi.org/10.1190/1.2431821

Huppert, H. E., Woods, A. W., 1995. Gravity-driven flows in porous layers. J. Fluid Mech. 292, 55–69.
URL http://journals.cambridge.org/abstract_S0022112095001431

Il'in, A., 1969. Differencing scheme for a differential equation with a small parameter affecting the highest derivative. Math. Notes Acad. Sci. 6 (2), 596–602.
URL http://link.springer.com/article/10.1007/BF01093706

IPCC, 2014. Climate Change 2014: Mitigation of Climate Change. Contribution of Working Group III to the Fifth Assessment Report of the Intergovernmental Panel on Climate Change. [Edenhofer, O., R. Pichs-Madruga, Y. Sokona, E. Farahani, S. Kadner, K. Seyboth, A. Adler, I. Baum, S. Brunner, P. Eickemeier, B. Kriemann, J. Savolainen, S. Schlmer, C. von Stechow, T. Zwickel and J.C. Minx (eds.)]. Cambridge University Press, Cambridge, United Kingdom and New York, NY, USA.
URL https://www.ipcc.ch/report/ar5/wg3/

Jones, D. W., Large, S., McQueen, A., Helmi, A., 2015. Reservoir geology of the Paleocene Forties Sandstone Member in the Fram discovery, UK Central North Sea. Geol. Soc., Lond., Spec. Pubs. 403 (1), 219–246.
URL https://doi.org/10.1144/SP403.13

Kilhams, B., Hartley, A., Huuse, M., Davis, C., 2015. Characterizing the Paleocene turbidites of the North Sea: Maureen Formation, UK Central Graben. Geological Society, London, Special Publications 403 (1), 43–62.
URL https://doi.org/10.1144/SP403.1

Lichtner, P., Karra, S., Hammond, G., Lu, C., Bisht, G., Kumar, J., Mills, R., Andre, B., 2015. PFLOTRAN user manual: A massively parallel reactive flow and transport model for describing surface and subsurface processes.

Tech. rep., Los Alamos National Laboratory (LANL).
URL http://dx.doi.org/10.2172/1168703

Lindeberg, E., Zweigel, P., Bergmo, P., Ghaderi, A., Lothe, A., 2001. Prediction of CO_2 distribution pattern improved by geology and reservoir simulation and verified by time lapse seismic. In: Conf. Greenh. Gas Contr. Tech. pp. 299–304.

Lüth, S., Ivanova, A., Kempka, T., 2015. Conformity assessment of monitoring and simulation of CO_2 storage: A case study from the Ketzin pilot site. Int. J. Greenh. Gas Control 42, 329–339.
URL https://doi.org/10.1016/j.ijggc.2014.08.011

Nilsen, H., Herrera, P., Ashraf, M., Ligaarden, I., Iding, M., 2011. Field-case simulation of CO_2-plume migration using vertical-equilibrium models. Energy Procedia 4, 3801–3808.
URL https://doi.org/10.1016/j.egypro.2011.02.315

Nilsen, H. M., Krogstad, S., Andersen, O., Allen, R., Lie, K.-A., 2017. Using sensitivities and vertical-equilibrium models for parameter estimation of CO_2 injection models with application to Sleipner data. Energy Procedia 114, 3476–3495.
URL https://doi.org/10.1016/j.egypro.2017.03.1478

Nilsen, H. M., Lie, K.-A., Andersen, O., 2016. Robust simulation of sharp-interface models for fast estimation of CO_2 trapping capacity in large-scale aquifer systems. Comput. Geosci. 20 (1), 93–113.
URL http://link.springer.com/10.1007/s10596-015-9549-9

Oldenburg, C. M., Mukhopadhyay, S., Cihan, A., 2016. On the use of Darcy's law and invasion-percolation approaches for modeling large-scale geologic carbon sequestration. Greenh. Gases Sci. Technol. 6 (1), 19–33.
URL http://doi.wiley.com/10.1002/ghg.1564

Peaceman, D. W., Rachford, H. H., 1955. The Numerical Solution of Parabolic and Elliptic Differential Equations. J. Soc. Indust. Appl. Math. 3 (1), 28–41.
URL http://www.jstor.org/stable/2098834

Pegler, S. S., Huppert, H. E., Neufeld, J. A., 2014. Fluid injection into a confined porous layer. J. Fluid Mech. 745, 592–620.
URL https://doi.org/10.1017/jfm.2014.76

Press, W. H., Flannery, B. P., Teukolsky, S. A., Vetterling, W. T., 2007. Numerical recipes 3rd edition: The art of scientific computing. Cambridge University Press.
URL http://numerical.recipes

Pruess, K., 1991. TOUGH2: A general-purpose numerical simulator for multiphase fluid and heat flow. Lawrence Berkeley Lab. Berekeley, California.
URL http://dx.doi.org/10.2172/5212064

Schlumberger, 2011. ECLIPSE technical description 2014. Tech. rep., Schlumberger Information Systems.
URL http://www.fanarco.net/books/reservoir/simulation/EclipseTechnicalDescripti

Singh, V. P., Cavanagh, A., Hansen, H., Nazarian, B., Iding, M., Ringrose, P. S., et al., 2010. Reservoir modeling of CO_2 plume behavior calibrated against monitoring data from Sleipner, Norway. In: SPE annual technical conference and exhibition. Society of Petroleum Engineers.
URL https://doi.org/10.2118/134891-MS

Smith, W. H. F., Wessel, P., 1990. Gridding with continuous curvature splines in tension. Geophysics 55 (3), 293–305.
URL http://library.seg.org/doi/10.1190/1.1442837

Vella, D., Huppert, H. E., 2006. Gravity currents in a porous medium at an inclined plane. J. Fluid Mech. 555, 353.
URL http://journals.cambridge.org/abstract_S0022112006009578

Williams, G. A., Chadwick, R. A., 2017. An improved history-match for layer spreading within the Sleipner plume including thermal propagation effects. Energy Procedia 114 (Supplement C), 2856–2870.
URL http://www.sciencedirect.com/science/article/pii/S1876610217315916

Zweigel, P., Arts, R., Lothe, A. E., Lindeberg, E. B. G., 2004. Reservoir geology of the Utsira Formation at the first industrial-scale underground CO_2 storage site (Sleipner area, North Sea). Geol. Soc. London, Spec. Publ. 233 (1), 165–180.
URL https://doi.org/10.1144/GSL.SP.2004.233.01.11